Chinese Chemical Letters 34 (2023) 107764

Contents lists available at ScienceDirect

Chinese Chemical Letters

journal homepage: www.elsevier.com/locate/cclet

Highly specific selenium nanosystems for fluorescent image-guided rapid diagnosis and pathological grading of ovarian malignant tumors

Shaolie Zheng[1], Wei Huang[1], Nan Li, Yuan Shen, Xiaoyu Wang*, Tianfeng Chen*

Department of Obstetrics & Gynecology, The First Affiliated Hospital of Jinan University, Guangzhou 510630, China

ARTICLE INFO

Article history:
Received 22 May 2022
Revised 12 August 2022
Accepted 18 August 2022
Available online 23 August 2022

Keywords:
Ovarian cancer
Selenium
Fluorescence imaging
Diagnosis
Pathological grading

ABSTRACT

Comprehensive surgical staging or optimal tumor cytoreductive surgery of malignant ovarian cancer directly affects disease prognosis. Therefore, a fluorescent selenium nanoparticle (Se@RGD/S2.2) decorated with cancer-targeting Arg-Gly-Asp (RGD) peptides and GCAGTTGATCCTTTGGATACCCTGG aptamer (S2.2) was developed for use as a diagnostic agent to achieve rapid, noninvasive diagnosis and visualization of microinvasive lesions during surgery for malignant ovarian cancer.

Ovarian cancer is one of the most common gynecologic malignancies and has the highest mortality rate among all gynecologic tumors [1–5]. At present, surgical intervention is a primary strategy for the treatment of ovarian cancer [6–8], and the residual disease (RD) size after surgery is directly associated with disease prognosis [9–14]. Thus, accurate identification of tumor lesions during ovarian cancer surgery is essential for complete cancer removal [15,16]. Developing a technique that allows effective intraoperative tumor visualization as a surgical guide may alleviate these issues [17–23].

Due to their unique advantages of high sensitivity and specificity, surface reconfiguration, and safety, nanotechnology-based imaging agents have been developed and may be used to efficiently enhance tumor diagnosis [24–28]. Because selenium (Se) is an essential trace element for humans, Se nanoparticles are excellent drug carriers that have been used in imaging-detection systems and have acquired unprecedented recognition [29,30]. Our group also previously prepared a cancer-targeted Se nano system that used Arg-Gly-Asp (RGD) as a targeting modifier and demonstrated its potential in the rapid visualization of bladder tumor tissues [31,32]. Within this Se nanosystem, the RGD polypeptide targeted tumor cells by recognizing overexpressed $\alpha_v\beta_3$ integrin receptors on the tumor cell membrane, making its targeting potential broad. Thus, the specificity of this system requires further refinement [33,34].

Studies have shown that the $\alpha_v\beta_3$ and cell membrane surface MUC1 are highly expressed in tumor cells. And the cyclic RGD peptide can better target $\alpha_v\beta_3$, a surface marker of tumor angiogenesis and metastasis. The MUC1 aptamer (GCAGTTGATCCTTTGGATACTGG) S2.2 can target the VNTR region of the tumor cell membrane surface marker TA-MUC1 [35–37].

Therefore, MUC1 and $\alpha_v\beta_3$ genes are highly expressed in ovarian cancer, based on Oncomine™ and TCGA database analysis and confirmed by IHC, and are, thus, important target molecules for rationally designing a nanosystem to specifically target ovarian cancer. Results in Fig. 1a show that among the 353 samples analyzed in the Oncomine™ database, 83 showed statistically significant differences in MUC1 expression and 54 had higher MUC1 expression in malignant ovarian tissue compared to nonmalignant ovarian tissue. Similarly, as shown in Fig. 1d, integrin-related ITGB3 showed statistically significant differences in 31 of the 459 samples analyzed. In addition, ITGB3 expression in tumor tissue was higher than that observed in nonmalignant ovarian tissue, as reported in 17 separate studies. In conclusion, mRNA expression of MUC1 and ITGB3 were increased in ovarian cancer.

The association of MUC1 and ITGB3 with ovarian cancer prognosis was analyzed using the TCGA database. As shown in Figs. 1b and e, MUC1 and ITGB3 were significantly overexpressed in ovarian cancer patients, consistent with the previous ONCOMINE database results. Additionally, as shown in Figs. 1c and f, overexpression of MUC1 and ITGB3 was associated with decreased patient survival, *i.e.*, overexpression of these genes reduced patient survival and led to poor prognosis in ovarian cancer patients.

* Corresponding authors.
E-mail addresses: twxy163@163.com (X. Wang), tchentf@jnu.edu.cn (T. Chen).
[1] These authors contributed equally to this work.

https://doi.org/10.1016/j.cclet.2022.107764
1001-8417/

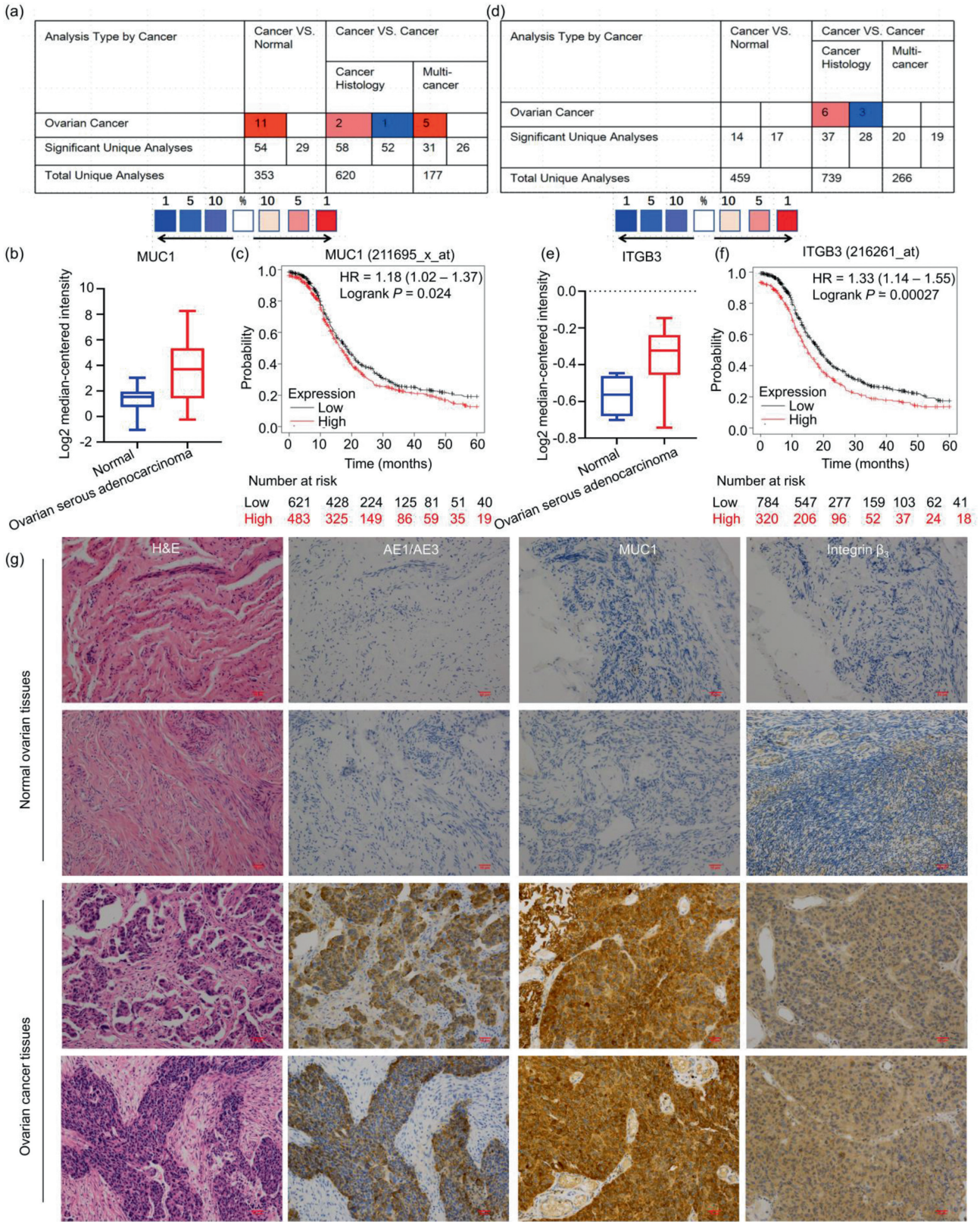

Fig. 1. Database analysis of Oncomine™ and TCGA to determine targeting peptide. (a, d) Transcriptional levels of MUC1 and ITGB3 mRNA in ovarian cancer with a threshold of *P*-value ≤ 0.01, fold change ≥ 2, and gene rank ≥ all gene. The data showed that the high expression (red) or low expression (blue) of MUC1 and ITGB3 mRNA represents the contrast between ovarian cancer and normal ovarian tissue. (b, e) The expression levels of MUC1 and ITGB3 mRNA in normal tissue and ovarian tumor. The data of (a), (b), (d) and (e) are all from Oncomine™ database. (c, f) The expression of MUC1and ITGB3 and ovarian cancer's survival data from the TCGA database. (g) Histological examination of normal ovarian tissue and ovarian tumor tissue from patients, scale bar = 10 μm.

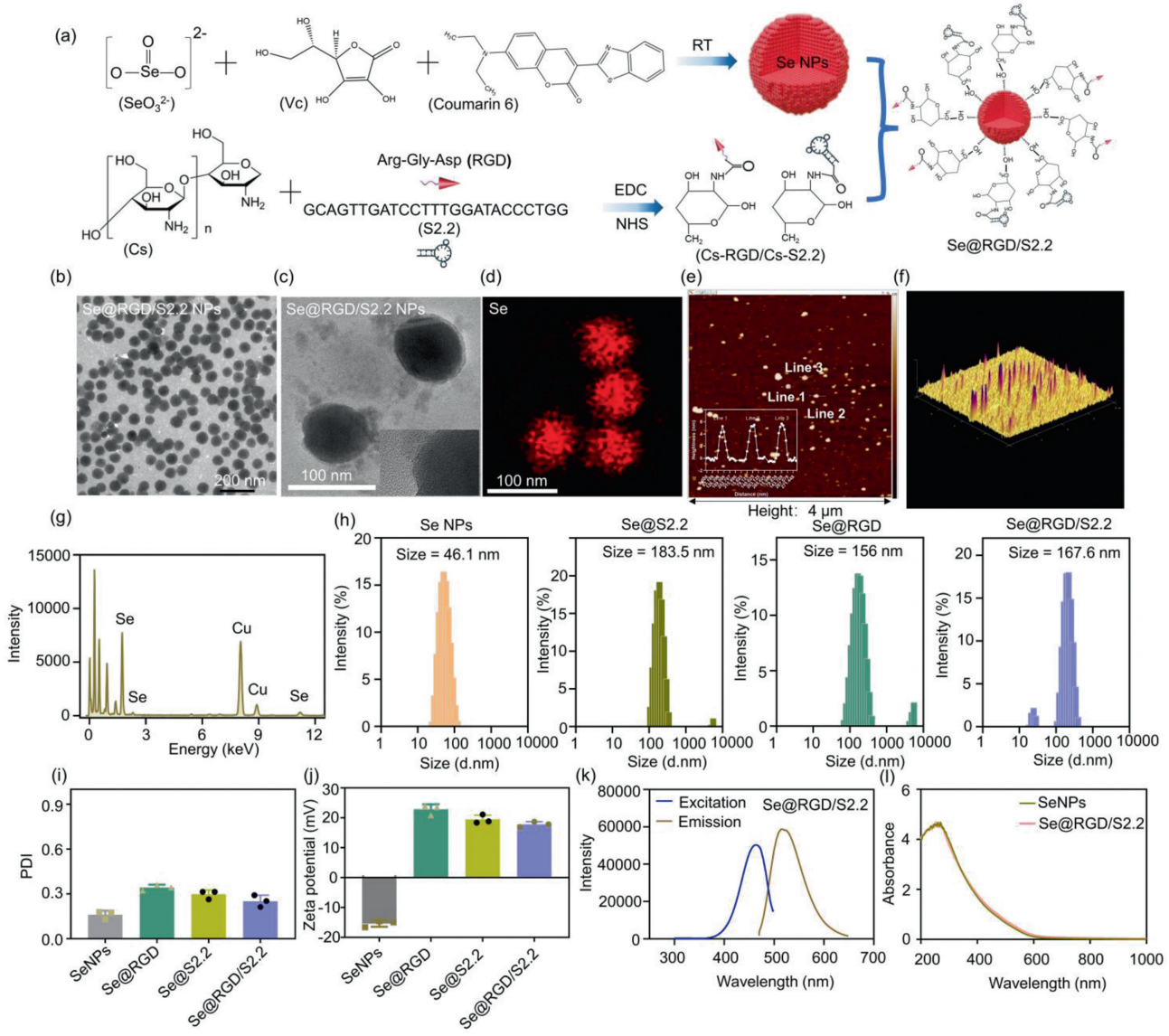

Fig. 2. (a) Proposed schematic illustration for synthesis of Se@RGD/S2.2 for fluorescent image-guided rapid diagnosis. (b, c) TEM images of Se@RGD/S2.2. (d) Mapping images of Se element. (e, f) AFM images and the 3D view of Se@RGD/S2.2. Inset: average height of Se@RGD/S2.2 along lines 1, 2 and 3 in Fig. 2e. (g) EDX analysis of Se@RGD/S2.2. (h) Size distributions of the SeNPs, Se@S2.2, Se@RGD and Se@RGD/S2.2 NPs. (i-j) PDI values and zeta potentials of these nanosystems. (k) Fluorescence spectrum of Se@RGD/S2.2. The excitation wavelength was 460 nm. (l) Ultraviolet absorption spectrum of SeNPs and Se@RGD/S2.2.

To prove that the highly expressed genes, integrin and MUC1, can be used as target genes of ovarian cancer, histological and immunological analyses of 25 ovarian tissue specimens was performed and tissues were classified according to the degree of benignity and malignancy. First, H&E staining was performed to determine histomorphology [38,39]. Compared with nontumor tissue, tumor tissue had abnormally enlarged nuclei, an increased number of pathological mitotic images, and increased nucleocytoplasmic ratios (Fig. 1g). The antibody AE1/AE3 reacts with cytokeratin CK1-8, 10, 14, 15, 16 and 19 is a broad-spectrum cytokeratin marker widely used to identify epithelia and epithelial-derived tumors and to determine whether metastatic tumors are epithelial-derived. Fig. 1g shows that the AE1/AE3 expression level is low in nontumor tissues and high in tumor tissues. Integrin and MUC1 IHC showed that integrin and MUC1 levels in normal tissues were much lower than those in tumor tissues, which was consistent with the results of H&E and AE1/AE3. Cellular immunofluorescence results show the $\alpha_v\beta_3$ and MUC1 gene higher express in ovarian cancer cells (A2780 and SKOV3) than those in normal cells IOSE80 (Fig. S1 in Supporting information). Collectively, these results suggest that $\alpha_v\beta_3$ integrin and MUC1 are highly expressed in ovarian cancer and may be selected as targeted molecules for the detection of ovarian cancer. The RGD peptide/S2.2, which could specifically bind to $\alpha_v\beta_3$ integrin/MUC1, has been chosen as the target molecule of the nanosystem for ovarian cancer diagnosis.

As shown in Fig. 2a, Se nanoparticles loaded with coumarin-6 (SeNPs) were synthesized using Na_2SeO_3 as the Se source and ascorbic acid (Vc) as the reducing agent, according to previously described methods [28]. Chitosan (Cs) connected RGD polypeptide and Cs connected S2.2 aptamer were then decorated to the SeNPs *via* electrostatic interactions to synthesize an ovarian cancer-target diagnostic system (Se@RGD/S2.2). Following preparation, the morphology and composition of Se nanosystem was characterized by atomic force microscopy (AFM) and transmission electron microscopy (TEM). As shown in Figs. 2b and c and Fig. S2 (Supporting information), SeNPs and Se@RGD/S2.2 exhibited uniform nanospheres with an average size of approximately 50 nm and 70 nm, respectively. Meanwhile, EDS elemental mapping analy-

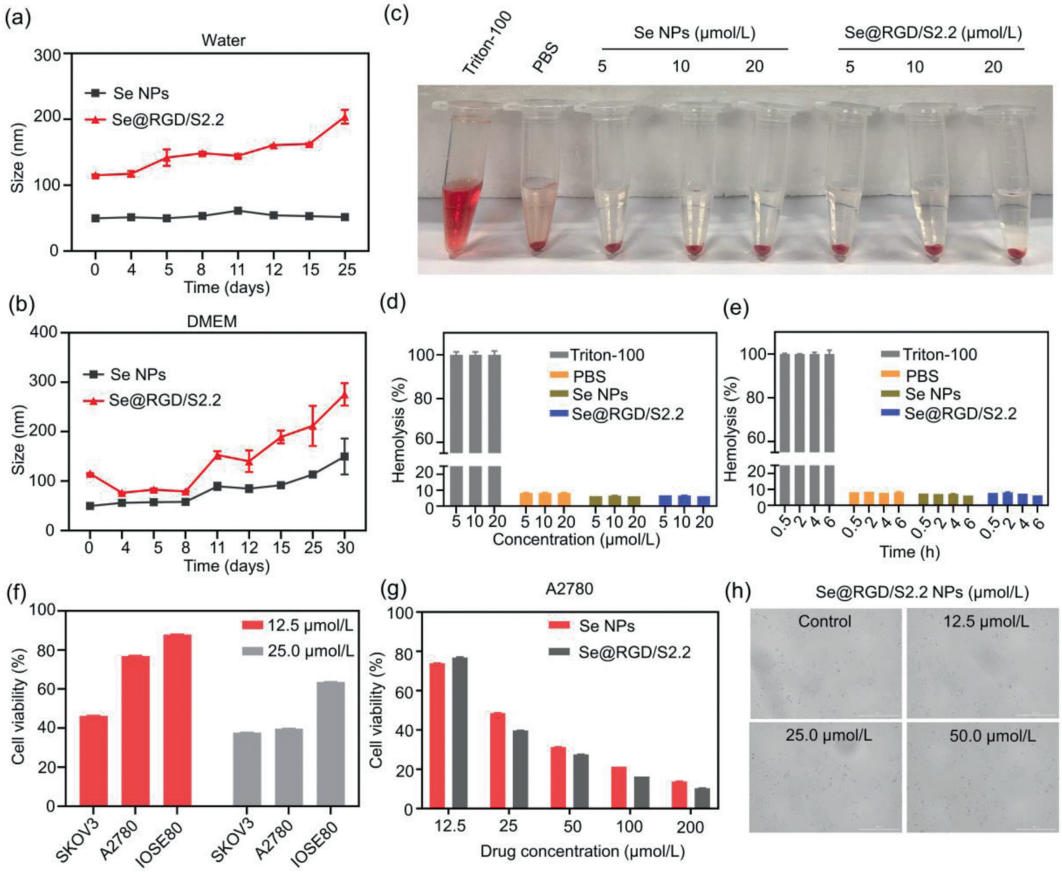

Fig. 3. Colloidal stability, hemcompatibility and cell viability assays. (a, b) The stability of the SeNPs and Se@RGD/S2.2 in water and DMEM solution. (c-e) Hemolytic analysis and corresponding photos of human red blood cells after incubation with SeNPs and Se@RGD/S2.2 for various times. (f, g) Viabilities of SKOV3, A2780 and IOSE80 after incubation with SeNPs and Se@RGD/S2.2 at various concentrations. (h) Photographs of IOSE80 cells treated with different concentrations of Se@RGD/S2.2 for 72 h.

sis showed that elemental Se was present in the Se@RGD/S2.2 nanosystem (Figs. 2d and g). Moreover, AFM images showed that Se@RGD/S2.2 was evenly distributed with an average height of approximately 30 nm (Figs. 2e and f). As shown in Figs. 2h–j, the hydrodynamic diameters and zeta potential of free SeNPs were 46.1 nm and −3.2 mV, respectively. After the surface of SeNPs was connected with RGD polypeptide/aptamer S2.2/RGD and S2.2 mixed peptides, the nanoparticle size was increased to 150–183 nm, and the zeta potential was reversed to positive charged, demonstrating the successful delivery of targeted peptides to the SeNPs. The fluorescence spectra of coumarin 6 showed that coumarin 6 exhibited green fluorescence at 530 nm when excited with at 334 nm wavelength (Fig. S3 in Supporting information). In addition, the fluorescence spectra of Se@RGD/S2.2 showed that Se@RGD/S2.2 exhibited green fluorescence at 530 nm when excited with at 460 nm wavelength, implying that Se@RGD/S2.2 successfully loaded coumarin-6 (Fig. 2k). Furthermore, Se@RGD/S2.2 and free SeNPs showed the same ultraviolet (UV) absorption peak, confirming that the structure of the Se nanosystem remained intact (Fig. 2l). Taken together, these results demonstrate that the Se@RGD/S2.2 nanosystem was successfully prepared.

The biocompatibility of nanosystems is an important parameter in considering their use in future medical applications. Hence, the stability of SeNPs in DMEM and PBS was determined by analyzing their size change. As shown in Figs. 3a and b, the SeNPs and Se@RGD/S2.2 nanosystem were stable in the water solution within 25 days. The particle size of the Se@RGD/S2.2 nanosystem in DMEM increased to approximately 250 nm, possibly due to the formation of a protein corona on the nanosystem. The hemcompatibility of Se@RGD/S2.2 was evaluated by calculating hemolytic rates, with Triton X-100 as a positive control and PBS as a negative control. Both SeNPs and Se@RGD/S2.2 caused inappreciable hemolysis, even at concentrations up to 20 μmol/L, indicating the excellent biocompatibility of Se nanosystems under physiological conditions (Figs. 3c–e). Furthermore, the MTT assay was used to investigate the toxicity of Se@RGD/S2.2 against tumor cells and nontumor cells. Following a 72 h incubation with Se@RGD/S2.2, SKOV3 and A2780 cancer cells exhibited lower viability than SeNP-treated cells (Figs. 3f and g). Se@RGD/S2.2 also exerted higher safety than SeNPs in nontumor human epithelial IOSE80 cells (Figs. 3f and g). Consistently, compared with the control group, complete IOSE80 cell morphology and number did not differ in response to varying Se@RGD/S2.2 concentrations (Fig. 3h). In order to reduce the influence of the high concentration of Se nanosystems on the absorption rate of normal cells and tumor cells, we selected the concentration of 10 μmol/L for subsequent cell experiments (Fig. S4 in Supporting information).

To investigate the ability of Se@RGD/S2.2 to enter cells, DAPI (blue fluorescence) and Lyso Tracker (red fluorescence) were used to label the nucleus and lysosomes, respectively. Se@RGD/S2.2 was mainly localized to the lysosomes in IOSE80 and A2780 cells (Figs. S5a-d in Supporting information), suggesting that lysosomes may play an important role in Se@RGD/S2.2 cell entry. More importantly, after 4 h of incubation, the green fluorescence signal in A2780 cancer cells was stronger than that in IOSE80 noncancer cells, supporting the ability of Se@RGD/S2.2 to specifically target cancer cells. To directly evaluate the ability of Se@RGD/S2.2 to target tumor cells, a cellular absorption assay *via* flow cytometry was performed. As shown in Figs. S5e-h (Supporting information), Se@RGD/S2.2 uptake in A2780 cancer cells increased in a time-

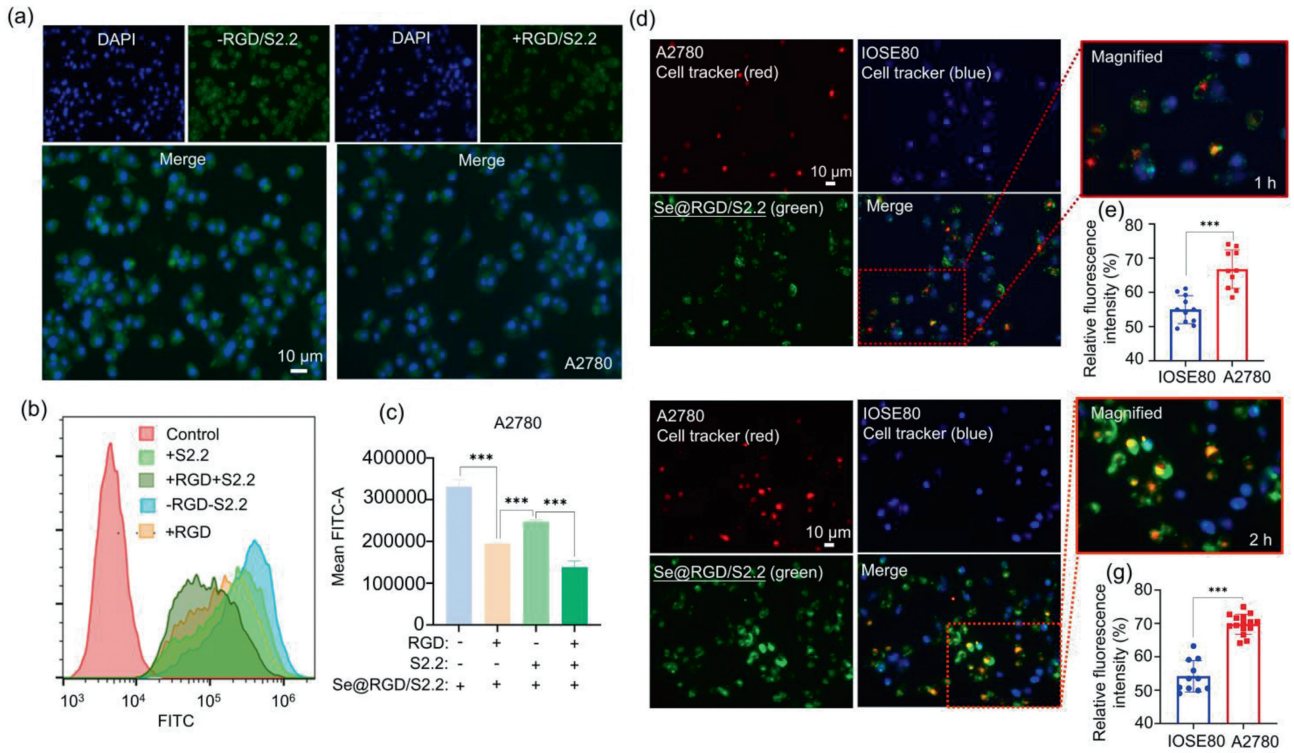

Fig. 4. The targeting of Se@RGD/S2.2 was verified by competition assay and co-culture model experiments. (a) Representative fluorescence images of A2780 cells with or without pre-incubation of RGD and S2.2 (1 mg/mL). (b, c) Flow cytometry examination of cellular uptake of A2780 cells after treated with RGD, S2.2, RGD/S2.2 for 1 h and then treated with Se@RGD/S2.2 for 2 h. After treatment with Se@RGD/S2.2 for 1 h (d, e) and 2 h (f, g) in the A2780/IOSE80 co-culture model, Fluorescence images and its corresponding statistical analysis. $^{***}P < 0.001$. Scale bar = 10 μm.

dependent manner and accumulated more quickly than Se NPs. Se@RGD/S2.2 accumulation time in IOSE80 cells showed no significant difference compared to Se NPs accumulation time. Thus, Se@RGD/S2.2 appears to be able to distinguish between noncancer and cancer cells but may not be able to clarify the functions of RGD and S2.2 polypeptides during endocytosis. Hence, A2780 cells were incubated with the same concentrations of Se@RGD, Se@S2.2 and Se@RGD/S2.2 for 1 h in subsequent experiments. Dual-targeted Se@RGD/S2.2 uptake in A2780 cells was significantly higher than that of the single-targeted Se nanosystem (Fig. S6 in Supporting information). Therefore, RGD and S2.2 may play indispensable roles in the selective absorption of Se@RGD/S2.2 in cancer cells.

To further demonstrate the specificity of RGD and S2.2 targeting, integrin and MUC1 competition assays using fluorescence microscopy and flow cytometric analysis were performed. As shown in Fig. 4a, the green fluorescence signal was decreased in A2780 cells preincubated with excess RGD and aptamer S2.2. Additionally, flow cytometry (Figs. 4b and c) showed that pretreatment with aptamer S2.2, RGD peptide or RGD polypeptide with aptamer S2.2, reduced intracellular uptake to 74.5%, 59% and 41.6%, respectively. These results collectively revealed that Se nanosystems enter ovarian cancer cells by inducing integrin and MUC1 receptors.

Furthermore, in order to compare the targeted ability of Se@RGD/S2.2 nanosystem more intuitively and accurately, IOSE80 cells labeled with Cell Tracker® Blue and A2780 cells labeled with Cell Tracker® Red were used to establish an IOSE80&A2780 cellular co-culture model. As expected, after 1-2 h of incubation, a significant overlap of green and red fluorescence was observed in A2780 cells, while green fluorescence was hardly observed in IOSE80 cells (Figs. 4d and f). Statistical analysis (Figs. 4e and g) of the fluorescence intensity showed that the absorption of Se@RGD/S2.2 in A2780 cells was approximately 2 times higher than that observed in IOSE80 cells. These results indicate that Se@RGD/S2.2 may selectively and specifically target ovarian cancer cells rather than noncancer cells. Based on these *in vitro* data, and guided by RGD and the S2.2 peptide, the Se@RGD/S2.2 nanosystem can accurately distinguish tumor cells with high expression of $\alpha_v\beta_3$ and MUC1 from nontumor cells with $\alpha_v\beta_3$ and MUC1 low expression. Hence, the Se@RGD/S2.2 nanosystem may be used as a diagnostic agent for the rapid diagnosis of ovarian cancer.

To explore whether the Se@RGD/S2.2 nanosystem could be used as a diagnostic agent for ovarian cancer tissues, histological staining was performed on 20 clinical tumor samples and 5 nontumor samples using Se@RGD/S2.2. All human tissue experiments were approved by the Ethics Committee of Human Experiments, Jinan University. Clinical specimens were legally and safely obtained from the First Affiliated Hospital of Jinan University. Detailed information of the 25 clinical tissue specimens is shown in Table S1 (Supporting information). Strong fluorescence signals were distinctly observed in ovarian cancer specimens treated with Se@RGD/S2.2 (Fig. 5a). In contrast, the nontumor tissue samples incubated with Se@RGD/S2.2 exhibited a weak fluorescent signal. These results demonstrate that Se@RGD/S2.2 is capable of staining clinical specimens and achieving a diagnosis of ovarian cancer.

At present, according to the WHO classification method, ovarian cancer is divided into four main stages (I, II, III, IV) [40]. Fluorescence analysis showed that Se@RGD/S2.2 had a targeted recognition effect on tumor metastasis (Fig. 5b). These results reveal that the fluorescence difference of the tissue specimens stained with Se@RGD/S2.2 can effectively distinguish cancerous from noncancerous tissue and determine the stage of ovarian cancer.

Comprehensive surgical staging or optimal tumor cytoreductive surgery of malignant ovarian cancer directly affects disease prognosis in patients. Unfortunately, identifying microinvasive lesions in adjacent noncancer tissue during surgery can be a challenging task for surgeons. Within the present study SeNPs were

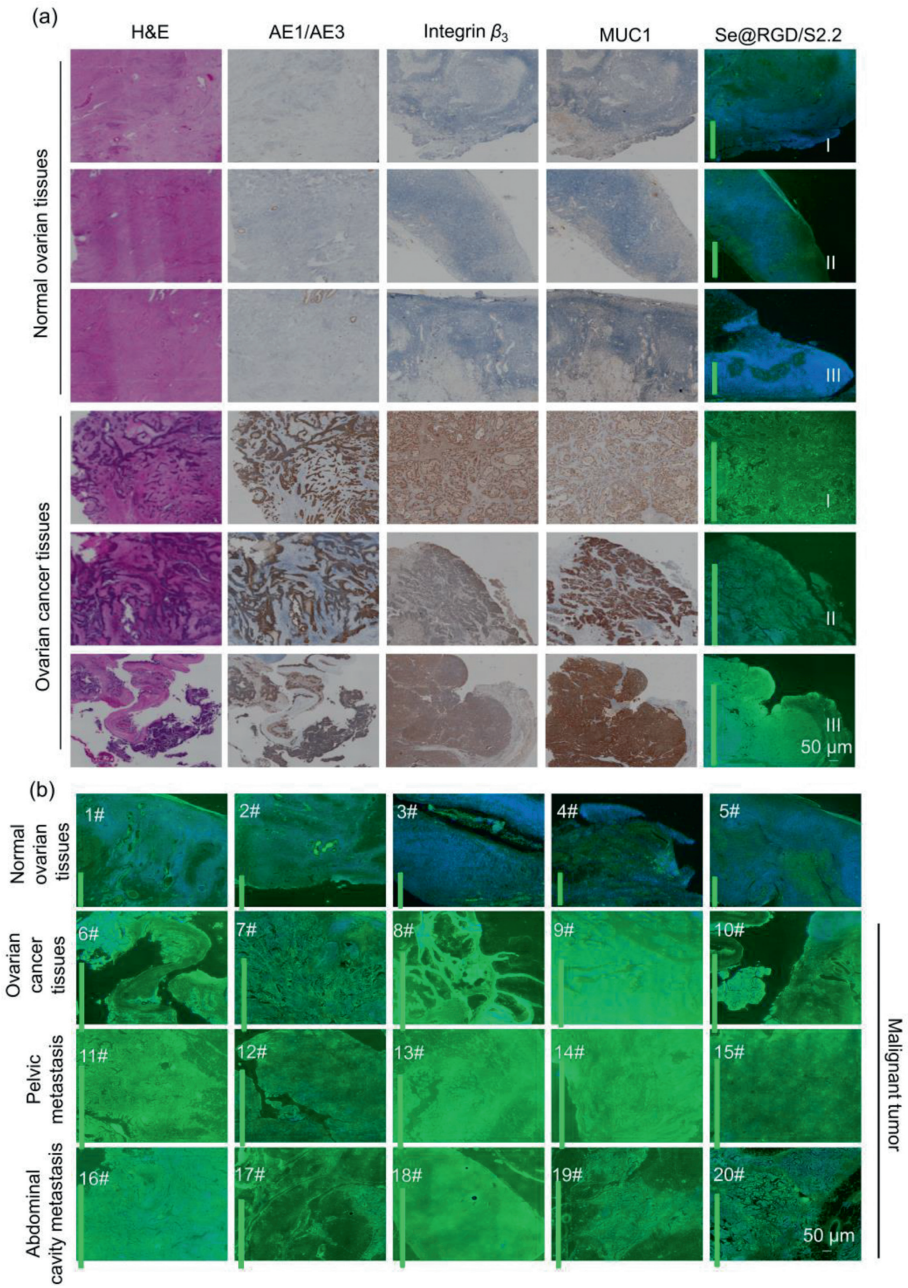

Fig. 5. Cancer diagnoses in different clinical specimens by using Se@RGD/S2.2. (a) Histological examination of normal ovarian tissues and ovarian cancer tissues, scale bar = 50 μm (H&E stained left column, AE1/AE3 second column, MUC1 and integrin β_3 right column). (b) Representative images of the diagnostic with Se@RGD/S2.2 (100 μmol/L) in different tissues (inset column represents the relative fluorescence intensity).

used as highly biocompatible carriers, with RGD and MUC1 as targeting peptides to synthesize the diagnostic agent Se@RGD/S2.2, based on the differential protein receptor expression on the cell membrane in ovarian cancer and noncancer tissues. Se@RGD/S2.2 was then used for visualization and pathological grading in clinical specimens of ovarian cancer. As expected, the rational design used in this study not only overcame the insufficiency of immunohistochemical reagents but also possessed the following advantages: (1) The nanosystem is easy to synthesize and has good blood compatibility and stability; (2) Possible target genes can be screened based on clinical databases, allowing a general strategy for nanodiagnostic agent and drug design in the future; (3) The high specificity of Se@RGD/S2.2 makes it more enriched in ovarian cancer cells, enabling it to distinguish noncancerous and cancerous tissues; (4) The nanosystem enables fast and convenient visualization of clinical tissue samples, which is expected to realize the integrated application of *in vivo* diagnosis and treatment in the future; (5) Pathological cancer grading was achieved using the fluorescence differential of Se@RGD/S2.2 in clinical tissue specimens. Thus, this study not only provides a simple and convenient strategy for the rapid and precise diagnosis of ovarian cancer but also provides new hope for clinical cancer theranosis.

Declaration of competing interest

The authors declare that they have no known competing financial interests or personal relationships that could have appeared to influence the work reported in this paper.

Acknowledgments

This work was supported by the National Natural Science Foundation of China (Nos. 21877049, 32171296), Guangdong Natural Science Foundation (No. 2020B1515120043), Major Program for Tackling Key Problems of Industrial Technology in Guangzhou (No. 201902020013), Innovation Team Project in Guangdong Colleges and Universities (No. 2019KCXTD008), Innovation Team Project in Guangdong Colleges and Universities (No. 2019KCXTD008) and Guangdong Basic and Applied Basic Research Fund Project (No. 2021A1515111027), the Fundamental Research Funds for the Central Universities (No. 21620310).

Supplementary materials

Supplementary material associated with this article can be found, in the online version, at doi:10.1016/j.cclet.2022.107764.

References

[1] E.I. Braicu, P. Wimberger, R. Richter, et al., J. Clin. Oncol. 38 (2020) TPS6102.
[2] R.L. Siegel, K.D. Miller, H.E. Fuchs, et al., CA Cancer J. Clin. 72 (2022) 7–33.
[3] S. Moufarrij, M. Dandapani, E. Arthofer, et al., Clin. Eplgenetcs 11 (2019) 7.
[4] A. Cho, V.M. Howell, E.K. Colvin, Front. Oncol. 5 (2015) 245.
[5] K.M. Su, H.W. Gao, C.M. Chang, et al., Biomedicines 9 (2021) 866.
[6] F.K. Albert, M. Forsting, K. Sartor, et al., Neurosurgery 34 (1994) 45–60.
[7] N. Colombo, C. Sessa, A. du Bois, et al., Ann. Oncol. 30 (2019) 672–705.
[8] L. Falzone, G. Scandurra, V. Lombardo, et al., Int. J. Oncol. 59 (2021) 53.
[9] W.E. Winter, G.L. Maxwell, C. Tian, et al., J. Clin. Oncol. 26 (2008) 83–89.
[10] S.J. Chang, R.E. Bristow, Gynecol. Oncol. 125 (2012) 483–492.
[11] S. Gu, S. Lheureux, A. Sayad, et al., Proc. Natl. Acad. Sci. U. S. A. 118 (2021) e2026663118.
[12] W.J. Tian, R. Jiang, X. Cheng, et al., J. Surg. Oncol. 101 (2010) 244–250.
[13] X.M. Fan, J. Zhang, S.H. Niu, et al., Int. J. Surg. 38 (2017) 61–66.
[14] M.C. Wouters, F.L. Komdeur, H.H. Workel, et al., Clin. Cancer Res. 22 (2016) 714–724.
[15] F.K. Albert, M. Forsting, K. Sartor, et al., Neurosurgery 34 (1994) 45–61.
[16] D. Yue, M. Wang, F. Deng, et al., Chin. Chem. Lett. 29 (2018) 648–656.
[17] R.M. Clark, L.W. Rice, M.G. Del Carmen, Gynecol. Oncol. 150 (2018) 370–377.
[18] Z. Xiao, H. Chen, H. Chen, et al., J. Biomed. Nanotechnol. 15 (2019) 1113–1134.
[19] H. Liu, W. Lin, L. He, et al., Biomaterials 226 (2020) 119545.
[20] A.L. Vahrmeijer, M. Hutteman, J.R. Van Der Vorst, et al., Nat. Rev. Clin. Oncol. 10 (2013) 507–518.
[21] B. Zhang, T. Tian, D. Xiao, et al., Adv. Funct. Mater. 32 (2022) 2109728.
[22] E.C. Pratt, M. Skubal, B. Mc Larney, et al., Nat. Biomed. Eng. 6 (2022) 559–568.
[23] L. Gong, L. Zhao, M. Tan, et al., J. Biomed. Nanotechnol. 17 (2021) 509–528.
[24] S.M. Park, A. Aalipour, O. Vermesh, et al., Nat. Rev. Mater. 2 (2017) 1–20.
[25] G. Huang, J. Zang, L. He, et al., ACS Nano 16 (2022) 431–452.
[26] L. He, G. Huang, H. Liu, et al., Sci. Adv. 6 (2020) eaay9751.
[27] L. Zhou, Y. Peng, Q. Wang, et al., J. Photoch. Photobio. B 167 (2017) 264–268.
[28] P. Valentini, R. Fiammengo, S. Sabella, et al., ACS Nano 7 (2013) 5530–5538.
[29] J.J. Wrench, C.I. Measures, Nature 299 (1982) 431–433.
[30] X. Xiao, Z. Shao, L. Yu, Chin. Chem. Lett. 32 (2021) 2933–2938.
[31] H. Liu, C. Mei, X. Deng, et al., Biomaterials 264 (2021) 120434.
[32] J. Li, H. Luo, X. Zhu, et al., Chin. Chem. Lett. 33 (2022) 788–792.
[33] C. Sang, L. Ma, D. Luo, et al., Chem. Eng. J. 371 (2019) 301–305.
[34] D. Li, L. Liang, Y. Tang, et al., Chin. Chem. Lett. 30 (2019) 1013–1016.
[35] Z. Liu, F. Wang, X. Chen, Drug Dev. Res. 69 (2008) 329–339.
[36] M.S. Nabavinia, A. Gholoobi, F. Charbgoo, et al., Med. Res. Rev. 37 (2017) 1518–1539.
[37] Y. Liu, G. Yang, T. Li, et al., Chin. Chem. Lett. 32 (2021) 1957–1962.
[38] W. Bulten, P. Bándi, J. Hoven, et al., Sci. Rep. 9 (2019) 1–10.
[39] M. Hou, Y. Zhong, L. Zhang, et al., Chin. Chem. Lett. 32 (2021) 1055–1060.
[40] S. Lheureux, M. Braunstein, A.M. Oza, CA Cancer J. Clin. 69 (2019) 280–304.